J Mol Model (2016) 22:258
DOI 10.1007/s00894-016-3123-9

ORIGINAL PAPER

Protein remains stable at unusually high temperatures when solvated in aqueous mixtures of amino acid based ionic liquids

Guillaume Chevrot[1] · **Eudes Eterno Fileti**[2] · **Vitaly V. Chaban**[2]

Received: 5 March 2016 / Accepted: 8 September 2016

Abstract Using molecular dynamics simulations, we investigated the thermal stability and real-time denaturation of a model mini-protein in four solvents: (1) water, (2) 1-ethyl-3-methylimidazolium alaninate [EMIM][ALA] (5 mol% in water), (3) methioninate [EMIM][MET] (5 mol% in water), and (4) tryptophanate [EMIM][TRP] (5 mol% in water). Upon analyzing the radius of gyration, the solvent-accessible surface area, root-mean-squared deviations, and inter- and intramolecular hydrogen bonds, we found that the mini-protein remains stable at 30–40 K higher temperatures in aqueous amino acid based ionic liquids (AAILs) than in water. This thermal stability was correlated with the thermodynamics and shear viscosity of the AAIL-containing mixtures. These results suggest that AAILs are generally favorable for protein conservation.

Keywords Protein · Ionic liquid · Molecular dynamics · Denaturation

Introduction

In order to investigate and understand the various physical and biological properties of proteins, it is necessary to extract them from their natural environment, separate them, and preserve without altering their structures [1–4]. This task is technically challenging, as most proteins are normally stable over a rather narrow range of conditions (temperature, pressure, pH, and solvent), and readily destabilize and precipitate otherwise [5, 6]. This feature largely prevents the existence of organisms—especially highly organized protein-based lifeforms—under extreme conditions. Many chronic diseases have been linked to incorrect folding states or instability of the tertiary/quaternary structures of key proteins [7].

Methods to preserve extracted proteins in vitro are currently being developed. The native three-dimensional structure of a protein depends on multiple hydrogen bonds as well as hydrophobic interactions. Furthermore, solvation of the polar amino acid residues by water and small inorganic ions stabilizes proteins and keeps the prospective binding sites hydrated. When proteins are damaged, most of the associated structural changes are irreversible due to the energy barriers between conformations and the potential for multiple similar conformations [8]. Computer simulations constitute a powerful and efficient tool [9–13] for probing the effects of different site–site interactions on protein stability and folding state [14–16], as well as the interplay between a few changes/mutations. Experimental methods (diffraction) of investigating a protein structure are less precise: they can determine folded structures, but not intermediate products and transition states.

Following protein extraction, certain alterations in temperature, pressure, and pH may lead to partial or full denaturation. For this reason, the role of the physicochemical properties of the solvent and its interaction with the protein are highly important. Amino acid based ionic liquids (AAILs) are a class of liquids that are derived from amino acids [17–20] and possess most of the properties that are characteristic of conventional ionic liquids (ILs), such as low volatility (and hence low vapor pressure), nonflammability, thermal stability, and straightforward tunability [21–24]. The ionic conductivities of AAILs are quite small, so their applicability as electrolytes is as yet

✉ Eudes Eterno Fileti
fileti@gmail.com

[1] Department of Physics, Chemistry and Pharmacy, MEMPHYS—Center for Biomembrane Physics, University of Southern Denmark, Odense, Denmark

[2] Instituto de Ciência e Tecnologia, Universidade Federal de São Paulo, 12231-280 São José dos Campos, SP, Brazil

Published online: 05 October 2016

unclear. This supposition is in accord with the results of experimental work by Ohno and coworkers, who reported fairly small ionic conductivities [20]. AAILs belong to the so-called third generation of ionic liquids, which are environmentally friendly. ILs were previously demonstrated to solvate proteins efficiently without incurring protein aggregation [8]. This feature implies that there is very favorable binding between proteins and ILs, although conformation of this assumption requires an appropriate atomically precise investigation. Since AAILs and proteins are genetically very close (both are derived from the alpha amino acids), a mutual affinity between them is expected (according to the principle that "like dissolves like"). AAILs may emerge as more suitable solvents for conserving proteins than water because (1) the carboxylate group is a stronger proton acceptor than water, (2) internal motions of AAILs are smaller than those of water at the same temperature, and (3) the normal boiling points of AAILs are systematically higher than that of water. AAILs are also infinitely miscible with water [18, 25].

In several recent works, ILs were positioned as alternative and promising solvents for protein assay and separation [26–35]. Chowdhury and coworkers reported a solvation dynamics study of the effect of an IL on the native and denatured states of a protein covalently attached to a probe [36]. Figueiredo and coworkers [37] argued that certain ILs are able to destabilize proteins and trigger their denaturation. This work utilized a combination of differential scanning calorimetry, nuclear magnetic resonance spectroscopy, and molecular dynamics (MD) simulations to achieve an atomically precise interpretation of specific interactions between proteins and ionic liquids. Takekiyo and coworkers studied the storage of lysozyme in an aqueous solution containing an ionic liquid and found that, when the concentration of the IL was too high, it induced structural alterations in the lysozyme [38]. Herrmann and coworkers [8] demonstrated that low-melting-point ILs effectively stabilize proteins and their enzymatic functions. Given the results of the works mentioned above, an exploration of the protein denaturation process in an IL in real time is deemed to be very important.

Therefore, in the work reported in the present paper, we employed classical equilibrium MD simulations and simulated annealing MD to identify and interpret the denaturation temperatures of a model mini-protein in three AAILs (each at a concentration of 5 mol% in water): 1-ethyl-3-methylimidazolium alaninate [EMIM][ALA], 1-ethyl-3-methylimidazolium methioninate [EMIM][MET], and 1-ethyl-3-methylimidazolium tryptophanate [EMIM][TRP]. Our recent publication [12] noted that storage in AAILs leads to higher thermal stability of the mini-protein. However, it is impossible to predict denaturation temperatures and mechanisms based on physiological temperature simulations. Therefore, here we report structural and thermodynamic properties of the solvated mini-protein as a function of temperature in order to explore the characteristics of the denaturation process in different AAILs. Furthermore, shear viscosities of the solvent mixtures were computed and compared to that of water.

Methods

The reported physical insights were obtained by performing classical MD simulations using pairwise atom–atom interaction potentials in the constant temperature and constant pressure ensemble. All chemical elements were represented explicitly. A time step of 2.0 fs, which was made possible by constraining covalent bond lengths involving hydrogen atoms (the LINCS algorithm) [39], was used when propagating the equations of motion. Periodic boundary conditions were simulated in all directions to represent an infinite system. The electrostatic interactions were simulated using Coulomb's law directly for interatomic separations of ≤1.2 nm and a computationally efficient implementation of the Ewald method (particle mesh Ewald) for separations >1.2 nm [40]. The Lennard-Jones interactions were shifted to zero from 1.0 to 1.2 nm using the switched-potential approach. The requested temperature (see below) was maintained using the Bussi–Donadio–Parrinello velocity rescaling thermostat [41] with a relaxation time of 0.1 ps. A constant pressure was maintained using the Parrinello–Rahman barostat [42] with a relaxation time of 1.0 ps and a compressibility constant of 4.5×10^{-5} bar^{-1}. The simulations were performed in GROMACS (version 5.0.5) [43–45]. The resulting molecular trajectories were analyzed by means of the GROMACS utilities. The molecular snapshots were prepared in the VMD (Visual Molecular Dynamics) software [46]. The initial configurations were prepared in PACKMOL [47].

We used entry #1L2Y from the Protein Data Bank (PDB) for the TRP-cage mini-protein. The CHARMM36 force field (FF) [48, 49] was employed to represent the mini-protein, and the recently developed CHARMM36-compatible FF [19, 50] was applied to represent AAILs. ILs are known to exhibit significant polarization effects, which were captured implicitly by the applied FF through point-charge manipulations. Extensive investigations of electronic polarization in ILs have been conducted by Kirchner and Borodin [51, 52]. One chloride anion was added to every MD system to achieve neutralization, since the mini-protein is positively charged, $q = +1e$.

At the preliminary stage, slow annealing simulations of the mini-protein in the 5 mol% [EMIM][ALA], [EMIM][MET], and [EMIM][TRP] aqueous mixtures were performed at 1 bar. The systems were heated from 310 K at two rates: 0.2 K ns^{-1} and 1.0 K ns^{-1}. It was concluded that both of these rates were slow enough not to introduce artifacts. Annealing has been successfully applied to protein simulations before [53]. The mini-protein and the solvent mixtures were T-coupled

separately and together to compare the effect. Separate T-coupling led to a 5–10 K difference in the resulting denaturation temperature, which is moderate given the accuracy of this work. Once the denaturation temperatures in the various AAILs were identified, the corresponding MD systems were simulated at these temperatures for 100 ns, saving the coordinates of each species every 10 ps. All reported properties were computed based on these 100-ns equilibrium simulations.

The radius of gyration (RG), root-mean-squared deviation (RMSD), solvent-accessible surface area (SASA), number of hydrogen bonds, and residues involved in the secondary structure (α-helix, β-sheet, β-bridge, and hydrogen-bonded turn, determined via the DSSP algorithm) were computed using the established procedures implemented in the GROMACS supplementary utilities (http://www.gromacs.org) [43–45]. To remove high-frequency components from the time dependencies of the structural properties of the mini-protein, the raw data were convoluted with a Gaussian function.

The shear viscosities were derived from a 10-ns nonequilibrium MD based on the energy dissipation of the system after introducing a cosine-shaped acceleration. The energy components were saved every 20 fs. The mathematical foundations and the benchmarks of this method have been outlined by Hess elsewhere [54]. The saturated vapor pressures were derived from the simulated liquid/vapor interfaces. In a 5 ns equilibration MD, the pressure was recorded every 10 fs. The unit cell dimensions were increased to 12 × 12 × 12 nm to accommodate vapor. The normal boiling point coordinates were, by definition, $p = 1$ bar and T ($p = 1$ bar).

Table 1 lists the simulated systems and their chemical compositions. The four systems p-water, p-ALA, p-MET, and p-TRP contained the mini-protein and were used to investigate the denaturation of the mini-protein upon heating (nonequilibrium MD) and during 100-ns equilibrium simulations at the predetermined denaturation temperatures. The other four systems, which did not contain the mini-protein, were s-water, s-ALA, s-MET, and s-TRP. These MD systems were used to investigate the physicochemical properties of the solvents (water and aqueous AAILs) in bulk form. The s systems were systematically smaller in number of interaction centers and volume.

Results and discussion

Upon slowly heating the mini-protein from 310 K, it loses its initial structure at a temperature termed the denaturation or unfolding temperature. This denaturation can be recorded precisely using the time dependences of the RMSD, SASA, and the number of hydrogen bonds. Figure 1 shows the simulated mini-protein at three points: (a) the physiological temperature (where its structure is identical to that obtained from the PDB); (b) the start of denaturation (the denaturation temperature); (c) when the denaturation is essentially complete. Significant structural alterations accompany denaturation; in particular, the globular shape of the mini-protein is lost in a series of steps. Note that the denaturation temperature corresponds to the beginning rather than the end of the denaturation process. We compared the denaturation process that occurred when heating the mini-protein in water at a rate of 0.2 K ns^{-1} to the processes that occurred when heating was carried out in the AAILs at 1.0 K ns^{-1}. There were essentially no differences in the structural alterations of the mini-protein during those processes. Therefore, it is clear that the selected heating rate is slow enough for the mini-protein to accommodate free-energy changes in its spatial structure. The selection of the heating rate is a key methodological consideration, as changing the rate can change the results both quantitatively and qualitatively.

The denaturation temperature depends on the solvent and AAIL species applied. Using the heating process described in the "Methods" section, we found that the denaturation temperature was 390 K in water, 420 K in the p-ALA system, 430 K in the p-MET system, and 430 K in the p-TRP system. Interestingly, denaturation occurred at the same temperature in p-MET and p-TRP, whereas it occurred at a temperature 10 K lower in p-ALA and 40 K lower in water—a significant difference. We can thus conclude that solvation in AAILs enhances the stability of the mini-protein. The remainder of the paper is devoted to our work investigating the molecular origin of this phenomenon.

It is obvious that the absolute values of the simulated denaturation temperatures are considerable overestimates; also,

Table 1 List of the simulated systems and their compositions

System name	AAIL	x (AAIL), mol%	No. of ion pairs	No. of water molecules	Comments
p-Water	—	0	0	5065	The p systems were used to simulate the annealing and thermal stability of the mini-protein
p-ALA	[EMIM][ALA]	5	300	5700	
p-MET	[EMIM][MET]	5	200	3800	
p-TRP	[EMIM][TRP]	5	200	3800	
s-Water	—	0	0	1140	The s systems were used to record the physicochemical properties of the solvent mixtures
s-ALA	[EMIM][ALA]	5	72	1368	
s-MET	[EMIM][MET]	5	66	1254	
s-TRP	[EMIM][TRP]	5	60	1140	

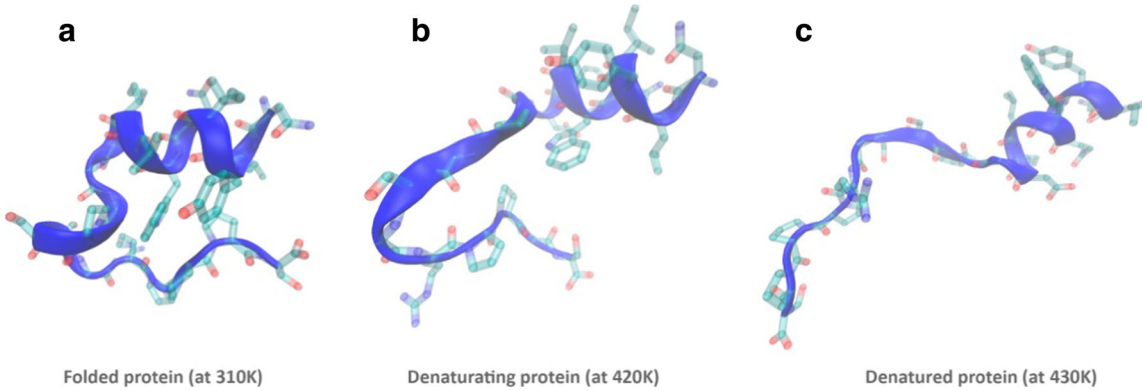

Fig. 1 Structures of the solvated mini-protein in the p-ALA system (Table 1): **a** folded, **b** denaturating, and **c** sufficiently denaturated. Solvent particles are omitted for clarity

the expected result in water is ca. 315 K. Such overestimated values from classical MD simulations are a known drawback of the widely and routinely used FFs [55]. These FFs were not calibrated for unfolding using thermodynamic data, i.e., the intraprotein interaction energies are likely biased. This is not critical for simulations at room temperature (although the results are still unrealistic), but it does lead to systematic error in cases like those of interest here. The resulting secondary and tertiary structures of the mini-protein appear to be excessively stable. In particular, the energetics of the intermolecular and intramolecular hydrogen bonding of the amide groups must be adjusted. Van Gunsteren and coworkers recently investigated this protein stability issue [55]. Much systematic research of this issue is required to refine the force fields.

Although the denaturation temperatures are shifted, our results still clearly indicate a difference in protein conservation between water and aqueous AAILs. Since the major source of overstabilization is intraprotein interactions (hydrogen bonds), the effect of the solvent can be isolated to some extent. The observed differences in the denaturation processes could be physically meaningful given that protein stability is strongly dependent on protein solvation. Therefore, in the following, we discuss denaturation temperature shifts rather than absolute denaturation temperatures.

Figure 2 depicts the radius of gyration (RG) vs. time. Structural stability of the mini-protein implies a static RG. Note that different solvents were simulated at different temperatures (390–430 K). As determined from the RG, denaturation of the mini-protein occurs in p-water within 50 ns; in p-ALA within 10 ns; in p-MET within 50 ns; and in p-TRP within 20 ns. Following the start of denaturation, the RG fluctuates heavily and increases somewhat. This is in line with Fig. 1, which shows the loss of the mini-protein's initial globular shape. The observed fluctuations in water (at 390 K) are systematically smaller than those in the AAILs (420–430 K). The frequency of the fluctuations depends on the dynamics of the particles (ions and molecules) in the solution, so it can be correlated with such properties as the self-diffusion coefficient and shear viscosity.

Root-mean-squared deviations are depicted in Fig. 3. The RMSD is the most widely used and likely most precise measure of structural deviations during thermal motion. Significant deviations in RMSD imply conformational changes and partial or complete loss of the initial structure. Conclusions drawn by studying the evolution of the RMSD during a simulation can be validated through visual analysis of the structures (Fig. 1). The changes in the RMSD point to the same denaturation times in all of the solvents as inferred from the changes in RG. These denaturation times are, however, poorly correlated with the physicochemical properties of the AAILs; for instance, it might be expected that p-MET would promote faster denaturation than p-TRP due to the smaller size of its anion and thus its higher mobility. Note that all starting conformations of the mini-protein and the solvent mixtures were taken from well-equilibrated systems at 310 K. Therefore, no initial perturbations were present.

The solvent-accessible surface area (Fig. 4) of the mini-protein increases when unfolding occurs and the solvent molecules can gain access to sites that were unavailable to them in the folded state. The fluctuations in the SASA are larger for

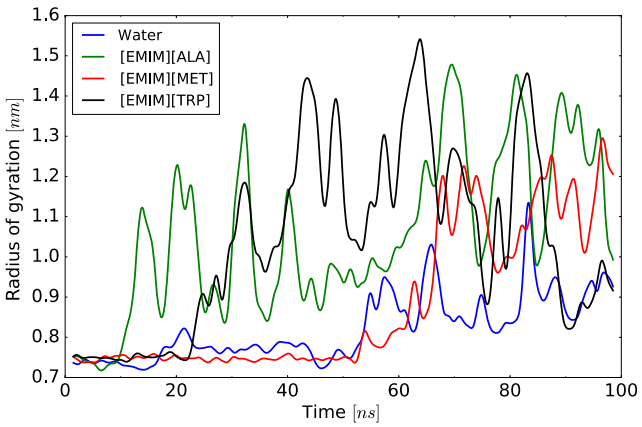

Fig. 2 Evolution of the radius of gyration of the mini-protein during 100-ns MD simulations in p-water, p-ALA, p-MET, and p-TRP (see also Table 1)

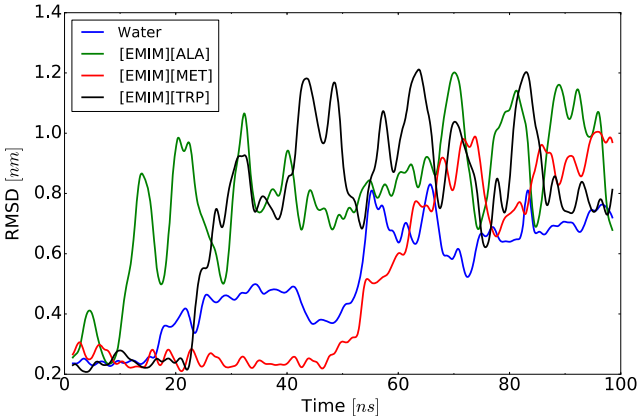

Fig. 3 Evolution of the RMSD of the mini-protein structure during 100-ns MD simulations in p-water, p-ALA, p-MET, and p-TRP (see also Table 1). An appropriately equilibrated mini-protein geometry at 310 K was used as the reference structure

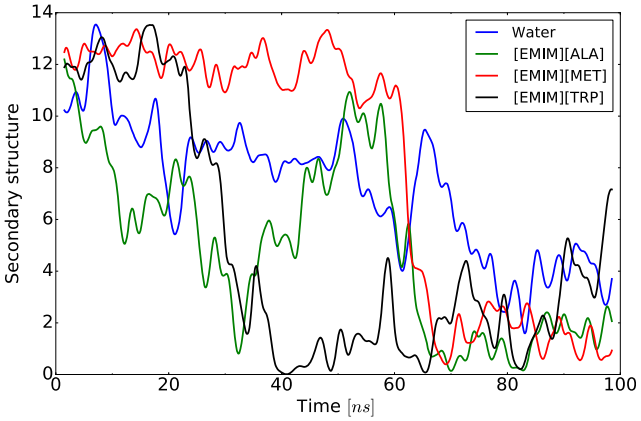

Fig. 5 Evolution of the total number of residues involved in the secondary structure (α-helices, β-sheets, β-bridges, and hydrogen-bonded turns) of the mini-protein during 100-ns MD simulations in p-water, p-ALA, p-MET, and p-TRP (Table 1)

the unfolded configurations than for the folded one. The increase in the SASA was found to be smaller in water than it is in the AAILs, leading us to hypothesize that the mini-protein unfolds to different states in water and in the aqueous AAILs due to different solvation and hydrogen-bonding patterns. However, further study of a series of unfolded mini-protein conformations is beyond the scope of our present work.

A loss of mini-protein secondary structure was indicated by a decrease in the total number of residues involved in the secondary structure (Fig. 5). This phenomenon occurred regardless of the solvent considered, and complete destruction of the secondary structure was observed by the end of each simulation (i.e., the number of residues involved in the secondary structure was zero, or close to zero). However, this destruction of the secondary structure occurred at various rates. Those rates did not correlate well with the types of amino acid residues present, but they did correlate well with the recorded time dependences of the properties discussed above. The agreement between the behavior of RG, RMSD, SASA, and degree of secondary structure during the simulations provides strong evidence of the denaturation event. Each of these structural properties is therefore an adequate descriptor of the simulated mini-protein denaturation.

To develop a hypothesis explaining the different solvation patterns of the mini-protein in water and the aqueous AAILs, we computed the numbers of intramolecular (Fig. 6) and intermolecular (Fig. 7) hydrogen bonds that participate in the solvation of the mini-protein-containing systems. The number of intermolecular hydrogen bonds in the stable mini-protein conformation is 4–5 times higher than the number of intramolecular hydrogen bonds. Furthermore, the number of intermolecular bonds with water molecules and ions increases from ~40 to ~50 (Fig. 7) whereas the number of intramolecular hydrogen bonds decreases irreversibly from ~12 to ~4 during the simulations. This clearly signifies a progressive unfolding of the coiled protein during the simulations, the protein–protein H-bonds being replaced with protein–solvent H-bonds. However, although the number of hydrogen bonds involving the mini-protein did fluctuate significantly over time, it remained essentially the same over the course of each simulation.

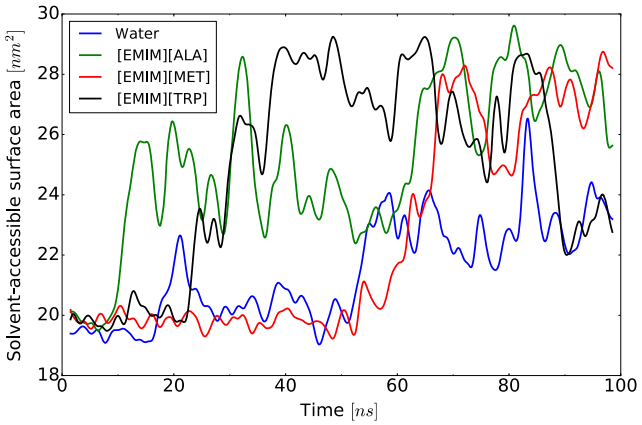

Fig. 4 Evolution of the SASA of the mini-protein structure during 100-ns MD simulations in p-water, p-ALA, p-MET, and p-TRP (see also Table 1)

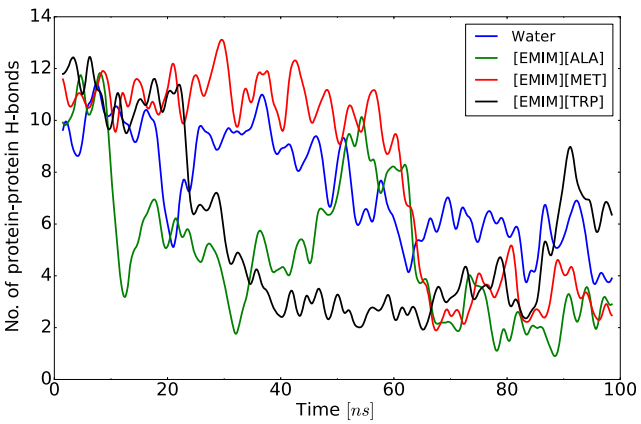

Fig. 6 Total number of protein–protein hydrogen bonds during 100-ns MD simulations in p-water, p-ALA, p-MET, and p-TRP (see also Table 1)

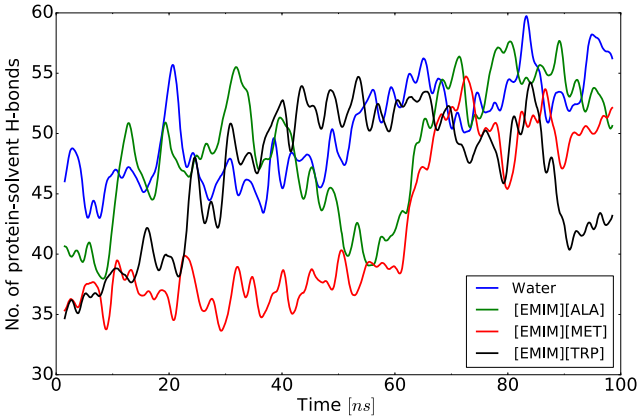

Fig. 7 Total number of protein–solvent hydrogen bonds during 100-ns MD simulations in p-water, p-ALA, p-MET, and p-TRP (see also Table 1)

The stability of the mini-protein and those of its conformations are determined by the balance between the protein–protein intramolecular interactions and the protein–solvent interactions. In turn, the ability of the solvent to solvate the protein is determined by the balance between the protein–solvent interactions and the solvent–solvent interactions (Table 2). We noticed that mini-protein solvation by AAIL is largely electrostatic in nature (this corresponds to 72–79 % of the total binding energy between the mini-protein and the AAIL). The van der Waals attraction (simulated using the classical Lennard-Jones (12,6) equation) is also quite significant (21–28 %). The fraction of binding energy corresponding to the Lennard-Jones interaction term increases from ALA to MET to TRP, in line with the increasing size of the hydrophobic moiety of the AAIL anion.

AAILs exhibit strongly electrostatic ion–ion binding (Table 2), wherein only 2.9–7.1 % of potential energy is attributed to the weak van der Waals attraction. The trend E(ALA) > E(MET) > E(TRP) seen for the protein–AAIL binding does not persist for the interionic attraction, wherein it becomes E(MET) > E(ALA) > E(TRP). This is a very interesting and largely unexpected observation, since the MET anion is larger than the ALA anion so it would be a natural to expect that the interionic attraction in p-MET is somewhat stronger than that in p-ALA. Indeed, the contribution from the van der Waals interaction is lower in p-MET than in p-ALA by 13 kJ mol^{-1} (Table 2), but the electrostatic contribution is higher by 19 kJ mol^{-1}. This fact implies that the ionic packing in [EMIM][ALA] is more energetically efficient [56], and is a strong indicator that the structure of the AAIL is not solely determined by the coordination of the carboxyl group of the anion to the imidazole ring of the cation [19].

Table 2 Coulombic and Lennard-Jones components of the total interaction energy between the protein and the AAIL and between ions (AAIL–AAIL). Percentages of the total interaction energy are given in parentheses

System designation	Potential energy, kJ mol^{-1}		
	Coulomb	Lennard-Jones	Total
Protein–AAIL, per mole of the protein			
p-ALA	−694 ± 41 (79 %)	−154 ± 8 (21 %)	−848 ± 49
p-MET	−929 ± 12 (75 %)	−286 ± 14 (25 %)	−1214 ± 26
p-TRP	−976 ± 25 (72 %)	−370 ± 4 (28 %)	−1346 ± 29
AAIL–AAIL, per mole of the AAIL ion pairs			
p-ALA	−679 ± 1 (97.1 %)	−20 ± 1 (2.9 %)	−699 ± 2
p-MET	−660 ± 1 (95.2 %)	−33 ± 1 (4.8 %)	−693 ± 2
p-TRP	−736 ± 1 (92.9 %)	−56 ± 1 (7.1 %)	−792 ± 2

The changes in the binding energies between the mini-protein and the AAILs over time in the simulations are provided in Figs. 8 and 9. The binding energies fluctuate strongly upon denaturation. However, it would be very difficult to accurately identify the time at which unfolding begins based on these plots, in contrast to plots of the other structural properties mentioned above. Thus, the folded and unfolded conformations of the simulated mini-protein show rather similar binding energies during solvation. This conclusion is reasonable, since solvation occurs due to favorable site–site attraction, whereas the conformation of the mini-protein is a complicated function of the inter- and intramolecular bonding characteristics.

A comparison of the ion–ion energies (Fig. 9) reveals that [EMIM][TRP] exhibits an interaction energy per mole of substance that is nearly 100 kJ mol^{-1} lower than those of [EMIM][ALA] and [EMIM][MET], which are very similar (indeed, the fluctuations in the energies of [EMIM][ALA] and [EMIM][MET] sometimes overlap).

The observed variations in mini-protein denaturation temperature depending on the solvent applied can be rationalized based on the physicochemical properties of the solvents. Figures 10 and 11 show the saturated vapor pressures and shear viscosities of the solutions of interest at 330–430 K. When the vapor pressure above the solution becomes

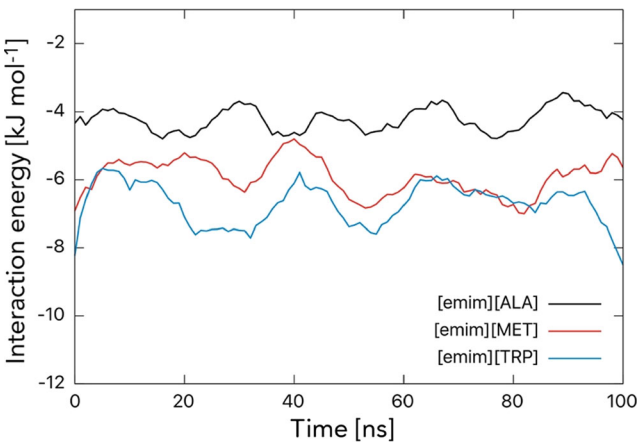

Fig. 8 Interaction energy between the mini-protein and each AAIL as a function of simulation time

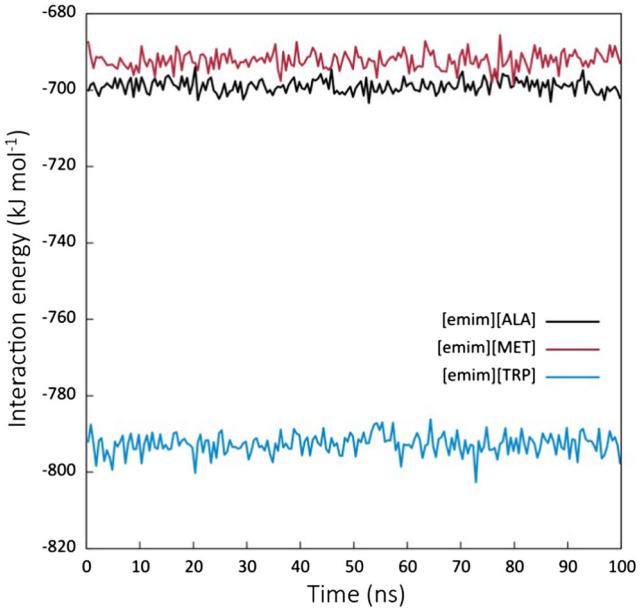

Fig. 9 Interaction energy between the AAIL ions in each simulated aqueous AAIL solvent

saturated, it can be used to determine the normal boiling point. All three AAIL-containing solutions (s-ALA, s-MET, and s-TRP) exhibit similar vapor pressures because their vapors contain only water molecules (the more volatile of the cosolvents). The organic ions do not vaporize due to their volumes and masses. The derived boiling points of the AAILs are all ca. 375 K. Accordingly, some of the water molecules leave the solution (making it richer in the AAIL), and are substituted by the ions in the mini-protein solvation shell. The AAIL–water mixtures can easily be distilled using this difference in boiling points. The similarity between the vapor pressures and between the boiling points of the AAILs explains the similarity between the denaturation temperatures of the mini-protein when solvated in them. Applying solutions richer in AAILs will likely lead to higher denaturation temperatures.

The TIP3P nonpolarizable model of water is reasonably successful at reproducing the normal boiling point in bulk

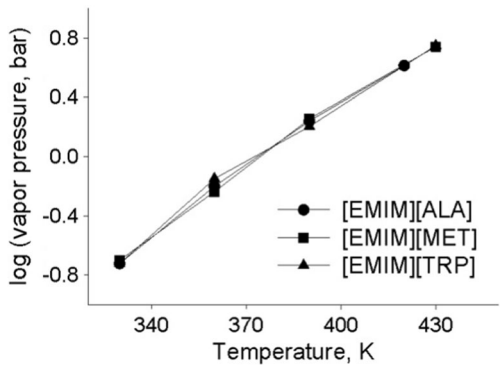

Fig. 10 Saturated vapor pressures above the AAIL solutions (5 mol% in water) vs. temperature

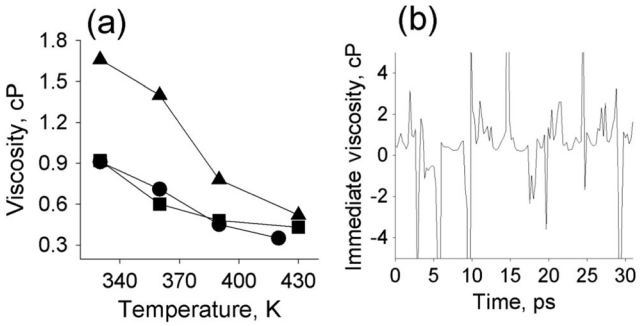

Fig. 11 **a** Shear viscosities of the AAIL solutions (5 mol% in water) vs. temperature. Computational uncertainties are commensurate with the size of the dots. *Circles* [EMIM][ALA], *squares* [EMIM][MET], *triangles* [EMIM][TRP]. *Connecting lines* are drawn to guide the eye. **b** Convergence and fluctuations in the computed viscosity of the cosine-accelerated system [EMIM][TPR] at 390 K

water. The result obtained, 365 K, is 8 K lower than the experimentally determined normal boiling point, 373 K. The saturated vapor pressures of water at other temperatures are 0.65 bar (360 K), 1.0 bar (365 K), and 1.3 bar (370 K). In the p systems, water exists in the form of a superheated liquid due to the simulation setup (no bubble formation, no space for a vapor phase).

Adding water to AAILs drastically decreases their viscosities (Fig. 11). 5 mol% mixtures of AAILs exhibit viscosities that are just 2–3 times higher than the viscosity of water, ca. 0.5 cP at 330 K. Increasing the temperature also substantially decreases the viscosity. The viscosities of the s-ALA and s-MET systems are similar, whereas the viscosity of the TRP system is 1.5–2.0 times higher. The mini-protein denatures at a solvent mixture viscosity of 0.3–0.5 cP. Denaturation in water occurs at a viscosity of 0.16 cP (390 K), whereas the viscosity at 420 K is only marginally lower, 0.14 cP. The low-viscosity environment present during denaturation is presumably a key factor in the denaturation process, since energy is dissipated and unfavorable fluctuations are spread across the mini-protein very quickly without being quenched. Figure 11b exemplifies the fluctuations in the immediate viscosity observed when sampling using molecular dynamics. In spite of the large fluctuations observed, the average viscosity under each simulated set of thermodynamic conditions is well defined. The standard error in the computed viscosity can be decreased by further increasing the sampling time.

Conclusions

Herein, we used classical MD simulations to study the thermal stability of a model mini-protein in four different solvents. The stability of the mini-protein stability was assessed in terms of RG, RMSD, SASA, number of residues involved in secondary structure, and number of hydrogen bonds. The denaturation temperatures and times were calculated in water and

5 mol% aqueous AAIL mixtures. When an AAIL was present in solution, the denaturation temperature of the mini-protein increased by 30-40 K.

This work showed, for the first time, that the denaturation time does not present a clear dependence on the AAIL species at the predetermined denaturation temperature, and that using AAILs instead of water enhances the thermal stability of the mini-protein.

Despite being good for simulating equilibrium protein structures, the CHARMM36 force field is not accurate enough to use to predict the absolute denaturation temperature of the simulated mini-protein. This is likely because the strengths of the intramolecular hydrogen bonds in the mini-protein are overestimated. Nonetheless, the computed differences in the denaturation processes that occur in water and the aqueous AAILs are physically meaningful because they significantly depend on the properties of the solvents and their solvation behaviors with respect to the mini-protein. It is reasonable to expect that 30–40 K higher denaturation temperatures will be calculated when a more accurate FF is developed for the mini-protein.

Acknowledgments E.E.F. and V.V.C. acknowledge FAPESP, CAPES, and CNPq.

References

1. Sari YW, Mulder WJ, Sanders JPM, Bruins ME (2015) Towards plant protein refinery: review on protein extraction using alkali and potential enzymatic assistance. Biotechnol J 10:1138–1157
2. Asenjo JA, Andrews BA (2011) Aqueous two-phase systems for protein separation: a perspective. J Chromatogr A 1218:8826–8835
3. Fabian C, Ju YH (2011) A review on rice bran protein: its properties and extraction methods. Crit Rev Food Sci Nutr 51:816–827
4. Zhu ZF, Lu JJ, Liu SR (2012) Protein separation by capillary gel electrophoresis: a review. Anal Chim Acta 709:21–31
5. Bratko D, Blanch HW (2001) Competition between protein folding and aggregation: a three-dimensional lattice-model simulation. J Chem Phys 114:561–569
6. Silva M, Figueiredo AM, Cabrita EJ (2014) Epitope mapping of imidazolium cations in ionic liquid–protein interactions unveils the balance between hydrophobicity and electrostatics towards protein destabilisation. Phys Chem Chem Phys 16:23394–23403
7. Boshette NB, Thakur KK, Bidkar AP, Trandafir C, Kumar P, Gogoi R (2014) Protein folding and misfolding in the neurodegenerative disorders: a review. Rev Neurol France 170:151–161
8. Weingartner H, Cabrele C, Herrmann C (2012) How ionic liquids can help to stabilize native proteins. Phys Chem Chem Phys 14: 415–426
9. Lane TJ, Shukla D, Beauchamp KA, Pande VS (2013) To milliseconds and beyond: challenges in the simulation of protein folding. Curr Opin Struct Biol 23:58–65
10. Chen CM (2000) Lattice model of membrane protein folding: Monte Carlo simulation of hydrophobic polypeptides. Biophys J 78:163a
11. Daggett V (2006) Protein folding—simulation. Chem Rev 106: 1898–1916
12. Chevrot G, Fileti EE, Chaban VV (2015) Enhanced stability of the model mini-protein in amino acid ionic liquids and their aqueous solutions. J Comput Chem 36:2044–2051
13. Chen J, Brooks CL (2008) Implicit modeling of nonpolar solvation for simulating protein folding and conformational transitions. Phys Chem Chem Phys 10:471–481
14. Huang LT, Gromiha MM (2008) Analysis and prediction of protein folding rates using quadratic response surface models. J Comput Chem 29:1675–1683
15. Jagielska A, Scheraga HA (2007) Influence of temperature, friction, and random forces on folding of the B-domain of staphylococcal protein A: all-atom molecular dynamics in implicit solvent. J Comput Chem 28:1068–1082
16. Koskowski F, Hartke B (2005) Towards protein folding with evolutionary techniques. J Comput Chem 26:1169–1179
17. Carlin C, Gordon MS (2015) Ab initio calculation of anion proton affinity and ionization potential for energetic ionic liquids. J Comput Chem 36:597–600
18. Chaban VV, Fileti EE (2015) Ionic clusters vs shear viscosity in aqueous amino acid ionic liquids. J Phys Chem B 119:3824–3828
19. Fileti EE, Chaban VV (2014) The scaled-charge additive force field for amino acid based ionic liquids. Chem Phys Lett 616:205–211
20. Ohno H, Fukumoto K (2007) Amino acid ionic liquids. Acc Chem Res 40:1122–1129
21. Chaban VV, Prezhdo OV (2013) Ionic and molecular liquids: working together for robust engineering. J Phys Chem Lett 4:1423–1431
22. Jordan A, Gathergood N (2015) Biodegradation of ionic liquids—a critical review. Chem Soc Rev 44:8200–8237
23. Mai NL, Ahn K, Koo YM (2014) Methods for recovery of ionic liquids—a review. Process Biochem 49:872–881
24. Wang XJ, Chi YL, Mu TC (2014) A review on the transport properties of ionic liquids. J Mol Liq 193:262–266
25. Dagade DH, Madkar KB, Shinde SP, Barge SS (2013) Thermodynamic studies of ionic hydration and interactions for amino acid ionic liquids in aqueous solutions at 298.15 K (vol 117, pg 1031, 2013). J Phys Chem B 117:9584
26. Patel R, Kumari M, Khan AB (2014) Recent advances in the applications of ionic liquids in protein stability and activity: a review. Appl Biochem Biotechnol 172:3701–3720
27. Chen XW, Mao QX, Wang JH (2013) Ionic liquids in extraction/separation of proteins. Prog Chem 25:661–668
28. Vasantha T, Attri P, Venkatesu P, Devi RS (2012) Structural basis for the enhanced stability of protein model compounds and peptide backbone unit in ammonium ionic liquids. J Phys Chem B 116: 11968–11978
29. Das DK, Das AK, Mandal AK, Mondal T, Bhattacharyya K (2012) Effect of an ionic liquid on the unfolding of human serum albumin: a fluorescence correlation spectroscopy study. ChemPhysChem 13: 1949–1955
30. Liu CC, Deng QL, Fang GZ, Liu HL, Wu JH, Pan MF, Wang S (2013) Ionic liquids monolithic columns for protein separation in capillary electrochromatography. Anal Chim Acta 804:313–320
31. Pei YC, Li ZY, Liu L, Wang JJ, Wang HY (2010) Selective separation of protein and saccharides by ionic liquids aqueous two-phase systems. Sci China Chem 53:1554–1560
32. Haberler M, Schroder C, Steinhauser O (2011) Solvation studies of a zinc finger protein in hydrated ionic liquids. Phys Chem Chem Phys 13:6955–6969
33. Attri P, Venkatesu P (2011) Thermodynamic characterization of the biocompatible ionic liquid effects on protein model compounds and their functional groups. Phys Chem Chem Phys 13:6566–6575
34. Jha I, Venkatesu P (2015) Endeavour to simplify the frustrated concept of protein–ammonium family ionic liquid interactions. Phys Chem Chem Phys 17:20466–20484
35. Rodrigues JV, Prosinecki V, Marrucho I, Rebelo LPN, Gomes CM (2011) Protein stability in an ionic liquid milieu: on the use of

differential scanning fluorimetry. Phys Chem Chem Phys 13: 13614–13616
36. Chowdhury R, Sen Mojumdar S, Chattoraj S, Bhattacharyya K (2012) Effect of ionic liquid on the native and denatured state of a protein covalently attached to a probe: solvation dynamics study. J Chem Phys 137:055104
37. Figueiredo AM, Sardinha J, Moore GR, Cabrita EJ (2013) Protein destabilisation in ionic liquids: the role of preferential interactions in denaturation. Phys Chem Chem Phys 15:19632–19643
38. Takekiyo T, Yamazaki K, Yamaguchi E, Abe H, Yoshimura Y (2012) High ionic liquid concentration-induced structural change of protein in aqueous solution: a case study of lysozyme. J Phys Chem B 116:11092–11097
39. Hess B, Bekker H, Berendsen HJC, Fraaije JGEM (1997) LINCS: a linear constraint solver for molecular simulations. J Comput Chem 18:1463
40. Darden T, York D, Pedersen L (1993) Particle mesh Ewald: an N·log(N) method for Ewald sums in large systems. J Chem Phys 98:10089–10099
41. Bussi G, Donadio D, Parrinello M (2007) Canonical sampling through velocity rescaling. J Chem Phys 126:014101–014108
42. Parrinello M, Rahman A (1981) Polymorphic transitions in single crystals: a new molecular dynamics method. J Appl Phys 52:7182–7192
43. Berendsen HJC, van der Spoel D, van Drunen R (1995) GROMACS—a message-passing parallel molecular dynamics implementation. Comput Phys Commun 91:43–56
44. Lindahl E, Hess B, van der Spoel D (2001) GROMACS 3.0: a package for molecular simulation and trajectory analysis. J Mol Model 7:306–317
45. Hess B, Kutzner C, van der Spoel D, Lindahl E (2008) GROMACS 4: algorithms for highly efficient, load-balanced, and scalable molecular simulation. J Chem Theor Comput 4:435
46. Humphrey W, Dalke A, Schulten K (1996) VMD: visual molecular dynamics. J Mol Graph 14:33–38
47. Martinez L, Andrade R, Birgin EG, Martinez JM (2009) PACKMOL: a package for building initial configurations for molecular dynamics simulations. J Comput Chem 30:2157–2164
48. Hatcher E, Guvench O, Mackerell AD Jr (2009) CHARMM additive all-atom force field for acyclic polyalcohols, acyclic carbohydrates and inositol. J Chem Theory Comput 5:1315–1327
49. Best RB, Zhu X, Shim J, Lopes PE, Mittal J, Feig M, Mackerell AD Jr (2012) Optimization of the additive CHARMM all-atom protein force field targeting improved sampling of the backbone phi, psi and side-chain chi(1) and chi(2) dihedral angles. J Chem Theory Comput 8:3257–3273
50. Fileti EE, Chaban VV (2015) The force field for imidazolium-based ionic liquids: novel anions with polar residues. Chem Phys Lett 633:132–138
51. Borodin O (2009) Polarizable force field development and molecular dynamics simulations of ionic liquids. J Phys Chem B 113: 11463–11478
52. Kirchner B, Hollóczki O, Canongia Lopes JN, Pádua AAH (2015) Multiresolution calculation of ionic liquids. Wiley Interdiscip Rev Comput Mol Sci 5:202–214
53. Agostini FP, Soares-Pinto DDO, Moret MA, Osthoff C, Pascutti PG (2006) Generalized simulated annealing applied to protein folding studies. J Comput Chem 27:1142–1155
54. Hess B (2002) Determining the shear viscosity of model liquids from molecular dynamics simulations. J Chem Phys 116:209–217
55. Gattin Z, Riniker S, Hore PJ, Mok KH, van Gunsteren WF (2009) Temperature and urea induced denaturation of the TRP-cage mini protein TC5b: a simulation study consistent with experimental observations. Protein Sci 18:2090–2099
56. Chaban VV, Fileti EE (2015) Mixtures of amino-acid based ionic liquids and water. J Mol Model 21:236